Geochimica et Cosmochimica Acta 361 (2023) 200–209

Contents lists available at ScienceDirect

Geochimica et Cosmochimica Acta

journal homepage: www.elsevier.com/locate/gca

Mercury abundance and isotopic composition in granitic rocks: Implications for Hg cycling in the upper continental crust

Zhendong Tian [a], Bernd Lehmann [b], Changzhou Deng [a], Anbo Luo [a], Xingchun Zhang [a], Frédéric Moynier [c], Runsheng Yin [a,*]

[a] State Key Laboratory of Ore Deposit Geochemistry, Institute of Geochemistry, Chinese Academy of Sciences, Guiyang 550081, China
[b] Mineral Resources, Technical University of Clausthal, 38678 Clausthal-Zellerfeld, Germany
[c] Université Paris Cité, Institut de Physique du Globe de Paris, CNRS, 1 rue Jussieu, Paris 75005, France

ARTICLE INFO

Associate editor: Sheng-Ao Liu

Original content: Supplementary Tables S1-S4 (Original data)
Supplementary Tables S1-S4 (Original data)

Keywords:
Mercury isotopes
Granite
Upper continental crust
Mass-independent fractionation

ABSTRACT

Mercury (Hg) is a highly volatile metal exhibiting both isotope mass-dependent (MDF, defined as δ^{202}Hg) and mass-independent (MIF, expressed as Δ^{199}Hg) fractionation. Assessing the Hg isotopic composition of the upper continental crust is crucial for the use of this new geochemical tool for petrogenetic tracing, particularly for understanding crust-mantle interaction. Here, we report Hg isotopic compositions of granitic rocks with distinct source affinity (I-, A-, and S-type) and of metasedimentary enclaves from the South China Craton. The results of more than 100 rock samples show large δ^{202}Hg variations of −2.03 to 0.47 ‰ and small Δ^{199}Hg variations of −0.16 to 0.09 ‰. The S-type granites studied here exhibit higher δ^{202}Hg values (−0.58 to 0.00 ‰; n = 57) than their sedimentary protoliths (metasedimentary enclaves; −2.03 to −0.91 ‰; n = 7), suggesting significant Hg-MDF during magmatic processes. The Δ^{199}Hg values of S-type granites (−0.08 to 0.09 ‰) are indistinguishable from their sedimentary protoliths (−0.16 to 0.02 ‰), suggestive of the absence of Hg-MIF during crustal anatexis and subsequent magmatic differentiation. The I- and A-type granites studied have smaller Δ^{199}Hg variations of −0.11 to 0.04 ‰ (n = 28) and −0.07 to 0.04 ‰ (n = 15), respectively, but are within the range of the S-type granites. The compositional range of all granite variants may be explained by the variable intensity of large-scale MASH (melting-assimilation-storage-homogenization) processes. Our new data combined with previously published data of igneous, sedimentary, and metamorphic rocks allow us to estimate that the upper continental crust (UCC) has a Hg abundance of 13.5 ppb and a weighted average δ^{202}Hg of −1.15 ± 1.01 ‰ (2SD), both of which are higher than the corresponding values of the primitive mantle. However, the weighted average Δ^{199}Hg value of the UCC (0.03 ± 0.15 ‰; 2SD) is nondistinguished from the primitive mantle, suggesting no obvious Hg-MIF during the formation and differentiation of the continental crust.

1. Introduction

Mercury (Hg) is a chalcophile and highly volatile element. It has seven natural stable isotopes (^{196}Hg, $^{198-202}$Hg, ^{204}Hg) and is the only metal displaying both significant isotope mass-dependent fractionation (MDF, defined as δ^{202}Hg, the permil deviation of the ^{202}Hg/^{198}Hg ratio relative to NIST SRM 3133 Hg standard) and mass-independent fractionation (MIF, generally expressed as Δ^{199}Hg) (Blum et al., 2014). While Hg-MDF is generated by various physical, chemical, and biological processes, Hg-MIF occurs mainly during photochemical reactions with little contribution from other processes (Bergquist and Blum, 2009; Estrade et al., 2009). Mercury sourced from the primitive mantle has near-zero Δ^{199}Hg (0.00 ± 0.10 ‰, 2SD) (Moynier et al., 2021), whereas photochemical processes on Earth's surface result in negative Δ^{199}Hg in the terrestrial system (−0.6 to 0 ‰, e.g., soil and vegetation) (e.g., Demers et al., 2013; Yin et al., 2013; Obrist et al., 2017; Woerndle et al., 2018; Sonke et al., 2023) and mostly positive Δ^{199}Hg in the oceanic system (−0.1 to 0.4 ‰, e.g., seawater and marine sediments) (Štrok et al., 2015; Yin et al., 2015; Meng et al., 2019; Kim et al., 2022; Yuan et al., 2023). As sedimentary, magmatic, metamorphic and hydrothermal processes do not produce Hg-MIF, Hg-MIF signals can be used as a diagnostic tracer of surface Hg cycling into deep reservoirs (Moynier et al., 2021; Chen et al., 2022; Yin et al., 2022). For instance, recent studies observed positive Δ^{199}Hg values in arc basalts (−0.01 to 0.34 ‰,

* Corresponding author.
E-mail address: yinrunsheng@mail.gyig.ac.cn (R. Yin).

https://doi.org/10.1016/j.gca.2023.09.019
Received 12 May 2023; Accepted 22 September 2023
Available online 28 September 2023

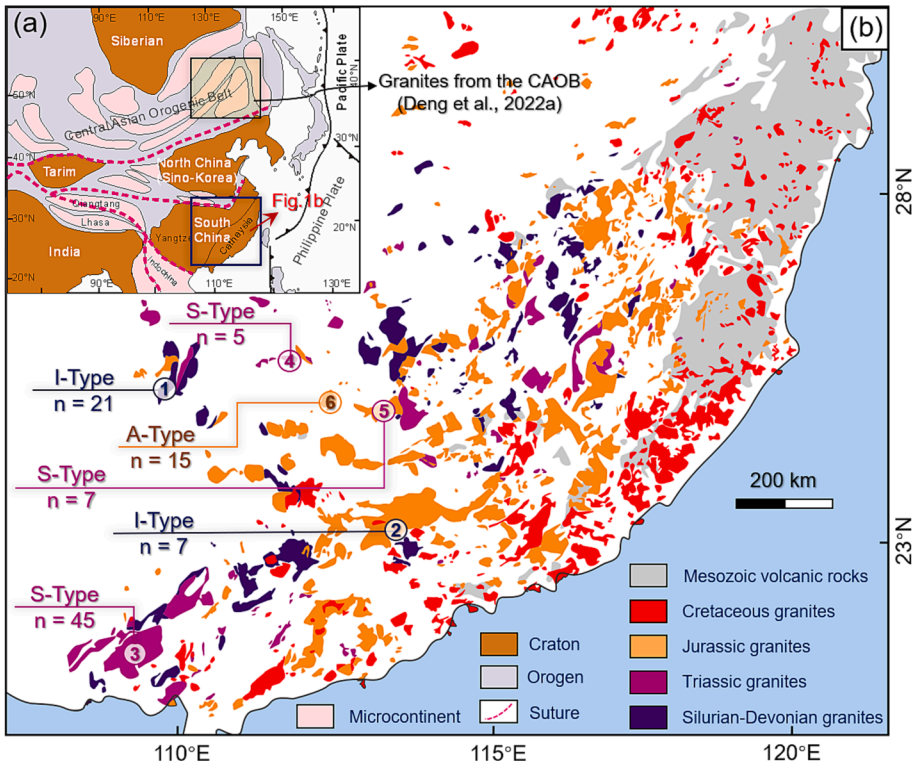

Fig. 1. (a) Simplified tectonic map of East Asia showing the distribution of cratons, orogens, and microcontinents (modified after Zhao et al., 2018). (b) Geographic distribution of the sampling sites, sample type, and number of samples studied. I-type granites were collected from the ~435 to 380 Ma Miaoershan-Yuechengling ① (n = 21) and the ~160 Ma Fogang batholiths ② (n = 7); S-type granites were collected from the ~250 Ma Shiwandashan-Darongshan batholith ③ (n = 45), ~220 Ma Tashan pluton ④ (n = 5), and Zhuguangshan complex ⑤ (n = 7); A-type granites are from the ~160 to 150 Ma Qitianling batholith ⑥ (n = 15). Granites from the Central Asian Orogenic Belt (CAOB) are from Deng et al. (2022a).

Yin et al., 2022), lamprophyres (−0.08 to 0.40 ‰, Wang et al., 2021), arc-related hydrothermal deposits (0 to 0.4 ‰, Deng et al., 2021) and HIMU-type lavas (0.23 ‰, Moynier et al., 2021), suggesting recycling of marine Hg into the mantle via oceanic plate subduction. On the other hand, the EM2-type lavas exhibit negative Δ^{199}Hg values (−0.14 to −0.02 ‰, Moynier et al., 2021), suggesting the recycling of terrestrial mercury into the Earth's mantle.

The Δ^{199}Hg signature of the oceanic crust has been studied through mid-ocean ridge basalts (0.01 to 0.22 ‰; Yin et al., 2022). However, the Δ^{199}Hg signature of the continental crust remains poorly constrained. Granitic rocks are the dominant constituents of the upper continental crust (UCC) (Wedepohl, 1995) and have been widely used to constrain the chemical composition of the UCC (Johnson et al., 2018; Hoefs, 2021). Several studies have shown a wider range of Δ^{199}Hg in granitic rocks (−0.23 to 0.21 ‰, Geng et al., 2018; Moynier et al., 2020; Deng et al., 2022a) than in mid-ocean ridge basalts, suggesting a more heterogeneous distribution of Hg isotopes in the UCC than in the oceanic crust. However, the geochemical behavior of Hg in the UCC and the

Table 1
Summary of lithology, age, and isotopic information of I-, S-, and A-type granites studied here.

Location	Exposed areas	Lithology	Mineral assemblages	Rock types	Age (Ma)	$\varepsilon_{Nd}(t)$	$\varepsilon_{Hf}(t)$	Data sources
Miaoershan-Yuechengling Batholith	~3400 km^2	Biotite granite/granodiorite	Amphibole, biotite, plagioclase, K-feldspar, quartz, and accessory minerals (e.g., zircon, apatite, titanite)	I-type	~435 to 380	−8.9 to −6.7	−9.5 to −4.0	Zhao et al., 2013
Fogang Batholith	~6000 km^2	Biotite monzogranite and syenogranite	Amphibole, biotite, plagioclase, K-feldspar, quartz, and accessory minerals (zircon, apatite, allanite, titanite, magnetite, ilmenite)	I-type	~160	−12.2 to −4.3	−11.5 to −3.1	Li et al., 2007
Shiwandashan-Darongshan Batholith	~10000 km^2	Hypersthene granite porphyry, hypersthene-cordierite-biotite granite	Plagioclase, quartz, and biotite, garnet, cordierite, hypersthene, and muscovite	S-type	~250	−14.1 to −9.9	−16 to −6	Qi et al., 2007; Hsieh et al., 2008
Tashan Pluton	~200 km^2	Two-mica monzogranite	Biotite, plagioclase, K-feldspar, quartz, muscovite, and accessory minerals (tourmaline, apatite, zircon, monazite, and Fe–Ti oxides)	S-type	~220	−9.9 to −12.2		Ma et al., 2016
Zhuguangshan Complex	~4000 km^2	Two-mica granite	Plagioclase, quartz, biotite, muscovite, and accesory minerals (zircon, apatite, titanite)	S-type	~160	−11.5 to −9.6	−15.7 to −11.8	Zhang et al., 2017; Lan et al., 2018
Qitianling Batholith	~520 km^2	Amphibole–biotite monzogranite and granodiorite	Plagioclase, quartz, biotite, amphibole, and accesory minerals (zircon, apatite, magnetite, titanite)	A-type	~160 to 150	−5.5 to −7.6	−8.1 to −3.7	Zhao et al., 2012a

reasons for the significant Hg isotopic heterogeneity in the UCC require further investigation.

It is worth noting that the available Hg isotope data on the UCC are mainly derived from I- and A-type granites formed by either fractional crystallization of mafic magma or partial melting of igneous protoliths (Chappell and White, 1974; Collins et al., 1982). So far, no Hg isotopic composition data for S-type granites, which were formed by partial melting of sedimentary rocks (Chappell and White, 1974), have been reported. The South China Craton offers a natural laboratory to study the fate of Hg in the UCC due to its vast exposure of granites covering 169,700 km^2 and its great diversity (I-, A-, S-type). Here, we analyze the Hg isotopic composition of 100 well-characterized granitic samples (including 28 I-, 57 S-, and 15 A-types) and 7 metasedimentary enclaves, representing the sedimentary protolith of the studied S-type granites. Our objectives are to (1) investigate Hg isotope behavior during crustal anatexis and magmatic differentiation, and (2) provide a preliminary estimate for Hg abundance and isotopic composition of the UCC.

2. Samples

The South China Craton (SCC) is a collage of the Yangtze and Cathaysia blocks, which amalgamated in the Neoproterozoic and have Archean roots (Zhai, 2015). The SCC hosts granitic rocks of different time series (~450 to 410 Ma, ~250 to 200 Ma, ~180 to 100 Ma) (Shu et al., 2021). These granitic rocks include I- and S-type granites whose protolith materials originated mainly from *meta*-igneous and *meta*-sedimentary rocks, respectively (Qi et al., 2007; Li et al., 2007; Hsieh et al., 2008; Zhao et al., 2013), as well as A-type granites formed under anorogenic and anhydrous conditions (Zhao et al., 2012a).

In this study, I-, S- and A-type granites were collected from six large granitic batholiths/complexes in the SCC (Fig. 1). Specifically, I-type granites were collected from the ~435 to 380 Ma Miaoershan-Yuechengling, and ~160 Ma Fogang batholiths; S-type granites were collected from the ~250 Ma Shiwandashan-Darongshan batholith, the ~220 Ma Tashan pluton, and the ~160 Ma Zhuguangshan complex; A-type granites were collected from the ~160 to 150 Ma Qitianling batholith. Seven samples of metasedimentary enclaves, representing the sedimentary protoliths of the Shiwandashan-Darongshan S-type granite (Zhao et al., 2012b), were also collected. The detailed petrological and geochemical characteristics of these six batholiths/complexes have been previously described in detail (see Supplementary Text S1 and references therein) and are briefly summarized in Table 1. The petrographic characteristics of these granites are shown in Fig. S1.

3. Analytical methods

The collected samples were inspected for any signs of weathering, crushed, and sieved to 200 mesh, prior to chemical analysis at the Institute of Geochemistry, Chinese Academy of Sciences (IGCAS).

Bulk rock major element analyses of the samples were performed at ALS Chemex Co., Ltd, China, using X-ray fluorescence spectrometry. Analytical uncertainty was better than 3 % for elements > 1 wt% and 10 % for elements < 1 wt%. Trace elements were measured by using an Agilent 7900 inductively coupled plasma mass spectrometry (ICP-MS) at IGCAS after hot HF-HNO_3 digestion (Qi et al., 2000), with an analytical uncertainty of better than 5 % for the trace elements reported.

Total Hg (THg) concentration and Hg isotopic compositions were analyzed at IGCAS. THg concentration was measured using a Lumex RA-915 + Hg analyzer equipped with a PYRO-915 + attachment (Russia), with a detection limit of 0.5 ng/g. Standard reference material GSS-4 (soil) was simultaneously tested to verify the data quality, which determined THg concentrations within ± 10 % of their certified value. Duplicate analysis of samples had an uncertainty of less than 10 %.

Following Hg concentration analysis, sample powders containing 10–25 ng Hg were processed using a double-stage tube furnace to pre-concentrate Hg in 5 mL of 40 % anti aqua regia (HCl/HNO_3 = 1/3, v/v) trapping solution (Huang et al., 2015). Standard reference material (GSS-4, soil; GSR-2, andesite) and method blanks were prepared in the same way as the samples. The former yielded Hg recoveries of 90–110 % and the latter showed Hg concentrations lower than the detection limit, precluding lab contamination. The preconcentrated solution was diluted

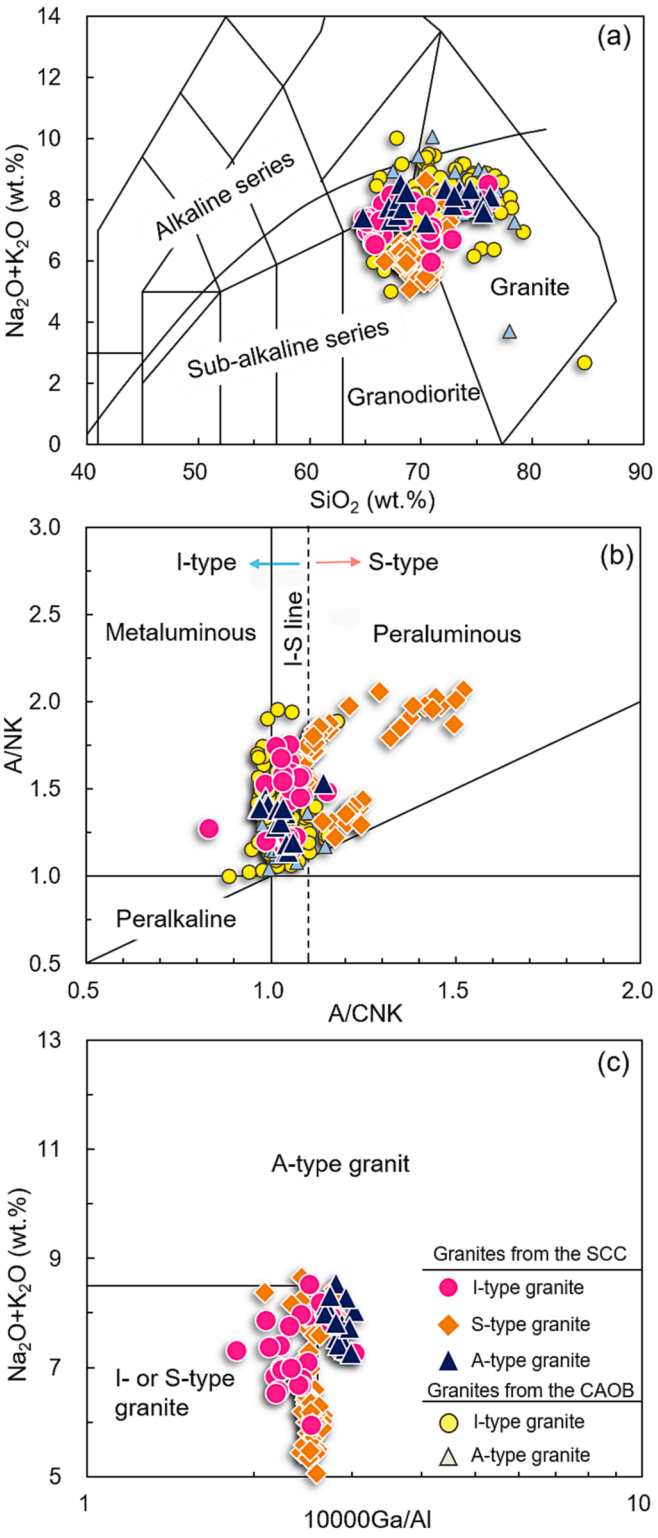

Fig. 2. (**a**) **SiO_2 versus Na_2O + K_2O** (after Middlemost, 1994), (**b**) **A/CNK versus A/NK** (after Maniar and Piccoli, 1989), and (**c**) **10000 Ga/Al versus Na_2O + K_2O** (after Whalen et al., 1987). A/CNK = molar $Al_2O_3/(CaO + Na_2O + K_2O)$, A/NK = molar $Al_2O_3/(Na_2O + K_2O)$.

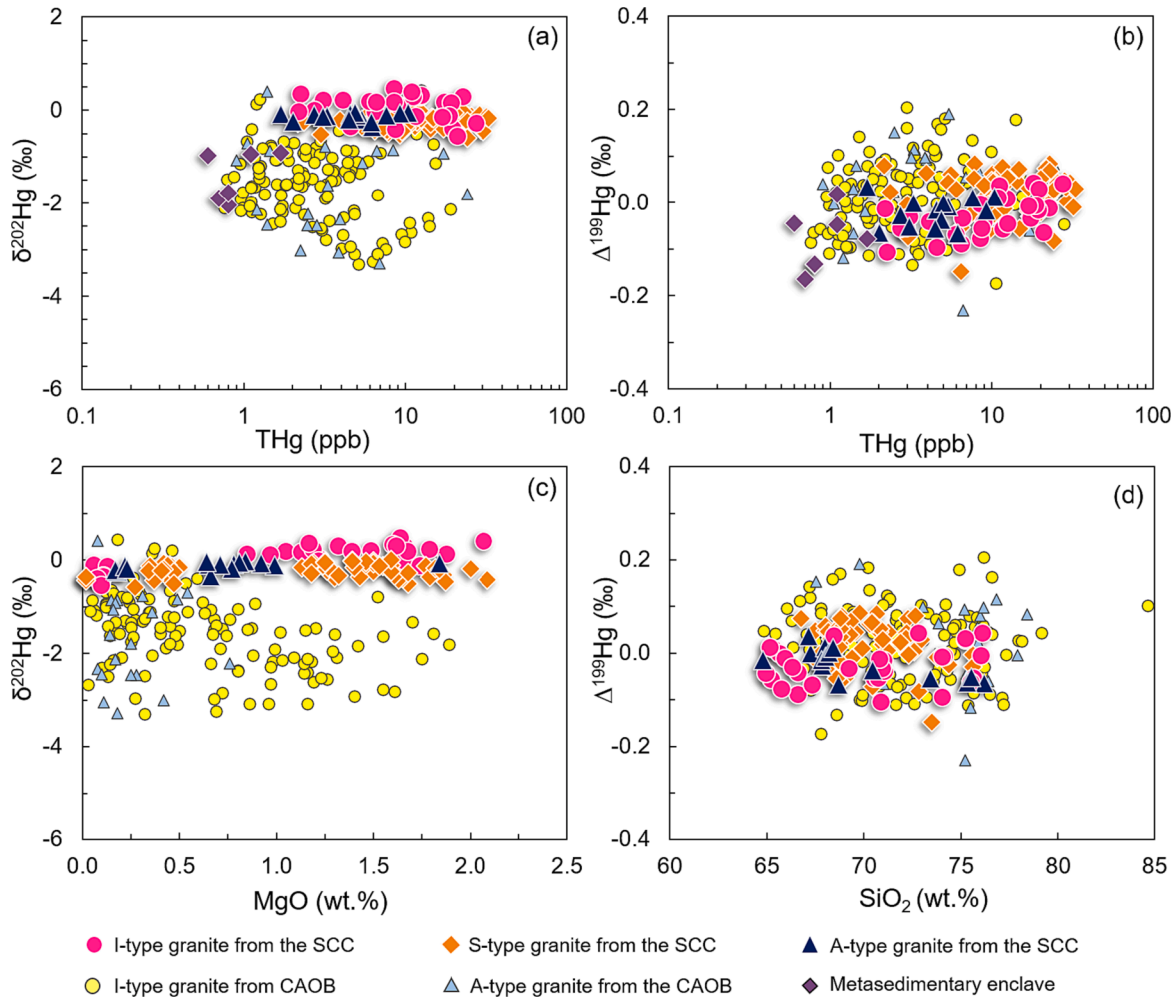

Fig. 3. (a) THg versus δ^{202}Hg, (b) THg versus Δ^{199}Hg, (c) MgO versus δ^{202}Hg, and (d) SiO_2 versus Δ^{199}Hg for the studied granites from the South China Craton (this study) and the Central Asian Orogenic Belt (CAOB) (Deng et al., 2022a); Analytical uncertainties (2SD) for δ^{202}Hg and Δ^{199}Hg are 0.11 ‰ and 0.06 ‰, respectively. Analytical uncertainty (RSD) for THg is < 10 %.

to 0.5 ng/mL with acid concentrations of 10–20 % before Hg isotope analysis using a Neptune Plus multi-collector inductively coupled plasma mass spectrometer (Yin et al., 2016). Briefly, the diluted Hg(II) solution was reduced to Hg(0) vapor via an online reaction with $SnCl_2$ solution. The resulting Hg(0) gas then was mixed with Tl aerosol generated by the Aridus II nebulizer and simultaneously introduced the plasma. The instrumental mass bias was corrected by the internal Tl standard (NIST SRM 997; $^{205}Tl/^{203}Tl = 2.38714$) as well as the standard-sample bracketing method using the NIST SRM 3133 Hg standard. Hg concentration and acid matrix in the bracketing NIST-3133 solutions were matched with neighboring samples. NIST 3177 secondary standard solution was measured every 10 samples to monitor the data quality. The data for Hg-MDF is expressed in δ^{xxx}Hg notation in units of ‰ referenced to the NIST-3133 Hg standard (analyzed before and after each sample):

$$\delta^{xxx}\mathrm{Hg}\ (‰) = \left[\left(^{xxx}\mathrm{Hg}/^{198}\mathrm{Hg}_{sample}\right)\Big/\left(^{xxx}\mathrm{Hg}/^{198}\mathrm{Hg}_{standard}\right) - 1\right] \times 1000 \quad (1)$$

where xxx refers to 199, 200, 201, or 202. By convention, δ^{202}Hg is used for the discussion of MDF. Hg-MIF is reported in Δ notation, which describes the difference between the measured δ^{xxx}Hg and the theoretically predicted δ^{xxx}Hg value, in units of ‰:

$$\Delta^{xxx}\mathrm{Hg} \approx \delta^{xxx}\mathrm{Hg} - \delta^{202}\mathrm{Hg} \times \beta \quad (2)$$

β is 0.2520, 0.5024, and 0.7520 for Δ^{199}Hg, Δ^{200}Hg and Δ^{201}Hg, respectively (Blum and Bergquist, 2007). The overall average and uncertainty of NIST-3177 (δ^{202}Hg = −0.57 ± 0.11 ‰; Δ^{199}Hg = −0.01 ± 0.06 ‰; Δ^{200}Hg = 0.02 ± 0.06 ‰; Δ^{201}Hg = −0.01 ± 0.05 ‰; 2SD, n = 15), GSR-2 (δ^{202}Hg: −1.60 ± 0.11 ‰; Δ^{199}Hg: 0.04 ± 0.03 ‰; Δ^{200}Hg: 0.00 ± 0.03 ‰; Δ^{201}Hg: 0.03 ± 0.07 ‰, 2SD, n = 3), GSS-4 (δ^{202}Hg: −1.66 ± 0.09 ‰, Δ^{199}Hg: −0.39 ± 0.05 ‰, Δ^{200}Hg: −0.02 ± 0.05 ‰; Δ^{201}Hg: −0.38 ± 0.06 ‰; 2SD, n = 3) are in accord with previous results (Estrade et al., 2010; Geng et al., 2018; Moynier et al., 2020; Yin et al., 2022). The largest values of standard deviation (2SD) for NIST-3177, GSR-2, and GSS-4 are used to indicate the 2 s analytical uncertainties, i.e. 0.11 ‰ for δ^{202}Hg, and 0.06 ‰ for Δ^{199}Hg.

4. Results

4.1. Whole-rock major and trace element composition

The granitic samples studied here are all fresh (Fig. S1), with low Chemical Index of Alteration (CIA: 45 to 60) and Loss on Ignition (LOI: typically < 2 wt%) values (Supplementary Table S1). They have SiO_2 contents ranging from 64.8 to 76.2 wt% and $Na_2O + K_2O$ contents of 5.06 to 8.65 wt%. In the total alkalis-silica diagram, most granitic samples fall into the field of granodiorite and granite (Fig. 2**a**). The studied I-type granites contain amphibole and are metaluminous to slightly peraluminous, with A/CNK (molar $Al_2O_3/(CaO + Na_2O + K_2O)$)

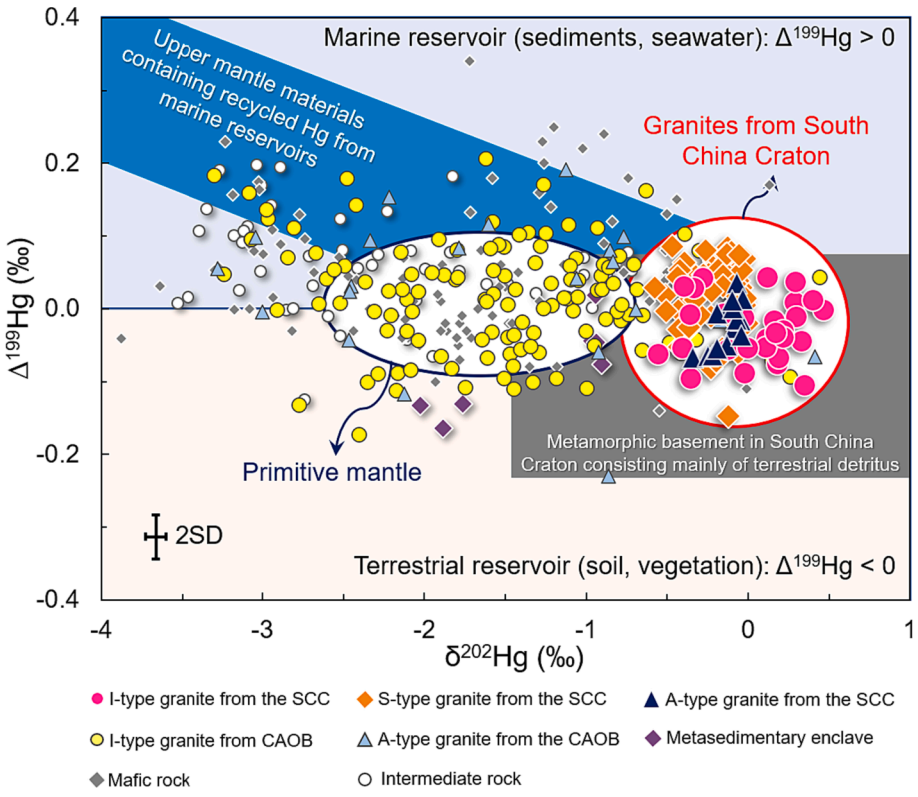

Fig. 4. Mercury isotope composition of granites from the South China Craton (SCC) and Central Asian Orogenic Belt (CAOB). Granitic rocks in the CAOB are from Deng et al. (2022a). The data of mafic rocks are from Geng et al. (2018), Moynier et al. (2020, 2021), Deng et al. (2022a), and Yin et al. (2022), intermediate rocks from Deng et al. (2022a). The light blue area represents the marine reservoirs (seawater and marine sediments) with positive Δ^{199}Hg values (Štrok et al., 2015; Yin et al., 2015; Meng et al., 2019; Kim et al., 2022; Yuan et al., 2023); the light pink area corresponds to the terrestrial reservoirs (soil and vegetation) with negative Δ^{199}Hg values (Demers et al., 2013; Yin et al., 2013; Jiskra et al., 2015; Zheng et al., 2016; Obrist et al., 2017; Woerndle et al., 2018; Liu et al., 2019; Sonke et al., 2023). The dark blue shaded areas represent subduction-related fluid metasomatized mantle that inherited positive Δ^{199}Hg signals from the oceanic system (Wang et al., 2021; Yin et al., 2022). The grey rectangular area represents the Hg isotope composition of Precambrian basement rocks in the SCC (Deng et al., 2022b). The white oval area denotes the Hg isotope composition of the primitive mantle (Moynier et al., 2021). Analytical uncertainties (2SD) for the data are 0.11 ‰ for δ^{202}Hg and 0.06 ‰ for Δ^{199}Hg.

values < 1.1 (Fig. 2**b**). The S-type granites are garnet- or muscovite-bearing (Fig. S1) and have A/CNK values > 1.1 (Fig. 2**b**). The A-type granites have variable aluminosity with A/CNK values of 0.97 to 1.14 **(**Fig. 2**b)**, and higher 10000 Ga/Al ratios (Fig. 2**c**) and high-field-strength-element (e.g., Nb, Ta, Zr, Hf) concentrations than I- and S-type granites (Supplementary Table S1).

4.2. Hg concentration

The analyzed granites have THg contents ranging from 1.70 to 32.8 ppb (Supplementary Table S2), within the range of previously reported values for felsic igneous rocks (0.76 to 42 ppb; Canil et al., 2015; Moynier et al., 2020; Deng et al., 2022a). Specifically, the I- and S-type granites studied show comparable THg variations of 2.19 to 27.5 ppb (11.3 ± 14.3 ppb, 2SD) and 2.17 to 32.8 ppb (14.8 ± 16.7 ppb, 2SD), respectively (Fig. 3**a**). The A-type granites have relatively low THg contents of 1.70 to 10.4 ppb, with a mean value of 5.11 ± 5.02 ppb (2SD). The seven metasedimentary enclaves have low THg contents (0.60 to 1.70 ppb) as well.

4.3. Hg isotopic composition

The studied granites exhibit a large variation of δ^{202}Hg (−0.58 to 0.47 ‰) and a small variation of Δ^{199}Hg (−0.15 to 0.09 ‰) (Fig. 4). Specifically, the I-type granites have δ^{202}Hg values varying from −0.56 to 0.47 ‰ (mean: 0.03 ± 0.56 ‰, 2SD) and Δ^{199}Hg values ranging from −0.11 to 0.04 ‰ (mean: −0.03 ± 0.08 ‰, 2SD). The S-type granites show δ^{202}Hg values of −0.58 to 0.00 ‰ (mean: −0.22 ± 0.30 ‰, 2SD) and Δ^{199}Hg values of −0.15 to 0.09 ‰ (mean: 0.02 ± 0.09 ‰, 2SD). The A-type granites display δ^{202}Hg and Δ^{199}Hg values of −0.34 to −0.03 ‰ (mean: −0.13 ± 0.18 ‰, 2SD) and −0.07 to 0.04 ‰ (mean: −0.02 ± 0.06 ‰, 2SD), respectively. THg contents, δ^{202}Hg, and Δ^{199}Hg values of all granites show no correlation with LOI and CIA values (Fig. 5), suggesting a limited influence of secondary alteration (e.g., weathering) on Hg contents and isotopic compositions (Nesbitt and Young, 1984; Lechler and Desilets, 1987). The seven metasedimentary enclaves have δ^{202}Hg values ranging from −2.03 to −0.91 ‰ (mean: −1.35 ± 1.03 ‰, 2SD) and Δ^{199}Hg composition ranging from −0.16 to 0.02 ‰ (mean: −0.08 ± 0.13 ‰, 2SD). All samples studied display a positive correlation between Δ^{201}Hg and Δ^{199}Hg, with a Δ^{199}Hg/Δ^{201}Hg ratio of 1.01 (Fig. 6), consistent with that observed during aqueous Hg(II) photoreduction (Δ^{199}Hg/Δ^{201}Hg ~1; Bergquist and Blum, 2007), but different from the Δ^{199}Hg/Δ^{201}Hg slope of ~1.6 to 2.0 during Hg evaporation and oxidation processes (Estrade et al., 2009; Ghosh et al., 2013; Sun et al., 2016).

5. Discussion

5.1. Estimation of Hg abundance in the upper continental crust

Early works, based on analysis of sediments, gave a variable average Hg content of the UCC ranging from 12.3 to 96 ppb (Taylor, 1964; Shaw et al., 1976; Wedepohl, 1995; Gao et al., 1998; Rudnick and Gao, 2003). A subsequent study, based on Hg concentrations of continental igneous

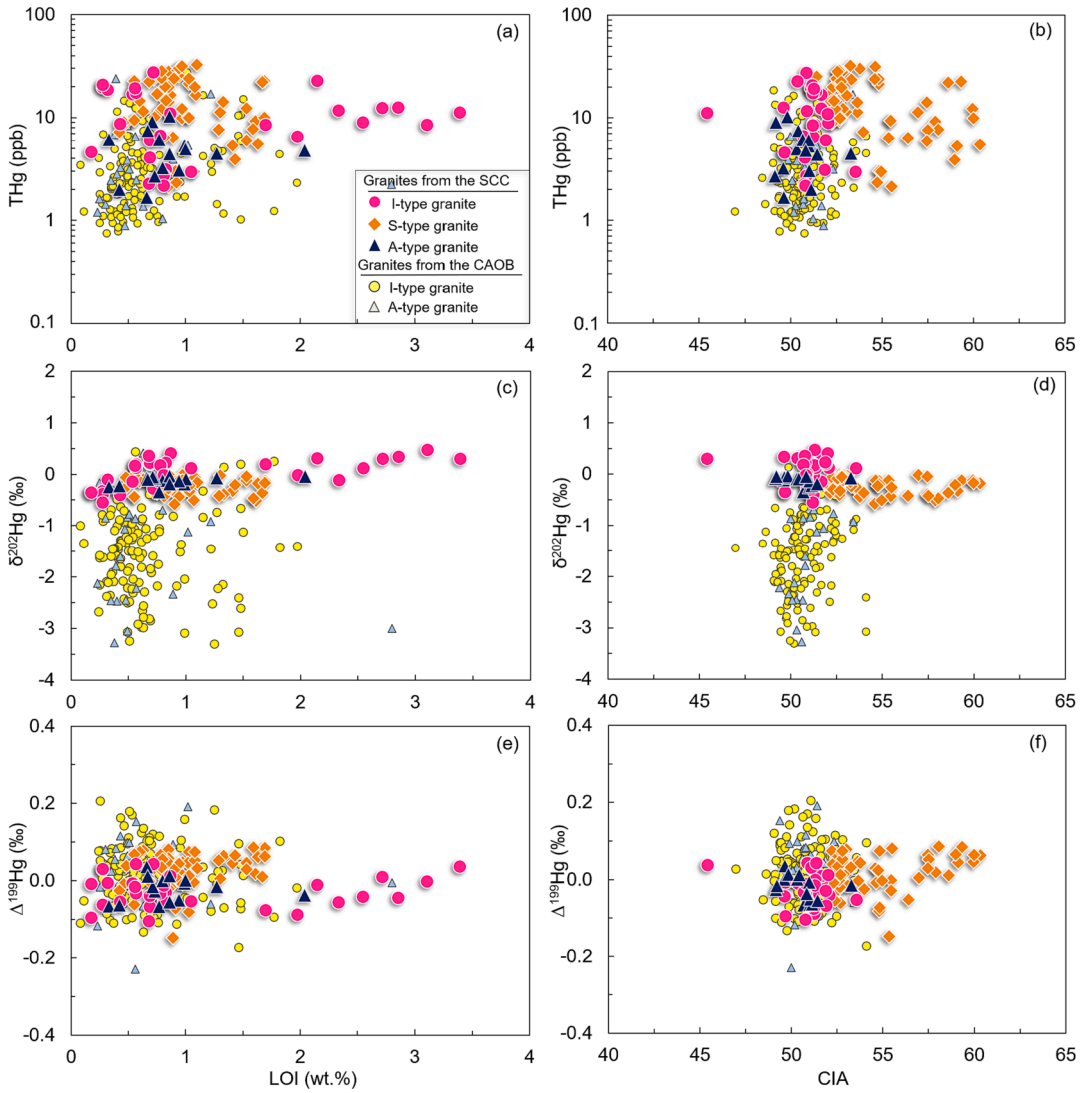

Fig. 5. Plots of (a) THg versus LOI, (b) THg versus CIA, (c) δ^{202}Hg versus LOI, (d) δ^{202}Hg versus CIA, (e) Δ^{199}Hg versus LOI, and (f) Δ^{199}Hg versus CIA for the studied granites from the South China Craton (this study) and Central Asian Orogenic Belt (CAOB) (Deng et al., 2022a). CIA = molar $Al_2O_3/(Al_2O_3 + CaO^*+Na_2O + K_2O) \times 100$, where CaO* represents Ca in silicate-bearing minerals only.

rocks, suggests a much lower Hg abundance of 2.9 ± 2.6 ppb for the UCC (Canil et al., 2015). The UCC is estimated to be comprised of six major rock units, including 14 % sedimentary rock, 25 % granite, 20 % granodiorite, 5 % tonalite, 6 % gabbro, and 30 % metamorphic rock (Wedepohl, 1995). By determining the average Hg content of each rock unit and by weighing it by its Hg abundance, the UCC can be calculated. This study, combined with previously published Hg contents of igneous and metamorphic rocks (Supplementary Table S3), yields average Hg contents of 7.88 ± 16.5 ppb for granite, 6.24 ± 9.52 ppb for granodiorite, 6.58 ± 8.18 ppb for tonalite, 8.65 ± 19.0 ppb for gabbro, and 2.16 ± 4.82 ppb for metamorphic rock (Table 2). These data, along with the estimated average Hg content of sedimentary rocks (62.4 ppb; Grasby et al., 2019), lead to a weighted average Hg abundance of 13.5 ± 17.8 ppb for the UCC. This value is lower than previously reported data (>50 ppb) by Taylor (1964), Shaw et al. (1976), Wedepohl (1995), and Rudnick and Gao. (2003), but consistent with the reported Hg content of UCC (12.3 ppb) by Gao et al. (1998) based on the analysis of 11,451 individual rock samples in East China. Compared to the Hg abundance for the oceanic crust based on MORB (1.36 ± 0.56 ppb) (Yin et al., 2022) and the mantle (0.4 to 0.6 ppb) (Canil et al., 2015), the UCC is enriched in Hg.

5.2. *Large δ^{202}Hg heterogeneity in the upper continental crust*

Hg-MDF occurs during a large variety of processes (Blum et al., 2014). The seven metasedimentary enclaves, representing the sedimentary protoliths of the studied S-type granites (Zhao et al., 2012b), have lighter δ^{202}Hg values (−2.03 to −0.91 ‰) than the S-type granites (−0.58 to 0.00 ‰). This confirms the previous proposal that igneous rocks should have heavier δ^{202}Hg values compared to their source rocks, due to the preferential loss of isotopically lighter Hg during magma degassing (Moynier et al., 2020).

I-, S-, and A-type granites studied, with mean δ^{202}Hg values of 0.03 ± 0.56 ‰ (2SD), −0.22 ± 0.30 ‰ (2SD), and −0.13 ± 0.18 ‰ (2SD), imply that the UCC of the South China Craton is enriched in heavier Hg isotopes, compared with the Central Asian Orogenic Belt (CAOB, Fig. 4), which exhibit much lower δ^{202}Hg of I-type granites (−1.56 ± 1.57 ‰, 2SD) and A-type granites (−1.60 ± 2.03 ‰, 2SD). The large δ^{202}Hg heterogeneity of granites between these two regions may be explained by different degrees of magmatic Hg degassing, given that Hg is highly volatile and is readily lost from the magmatic system via Hg degassing with the enrichment of lighter δ^{202}Hg in volcanic gas (Zambardi et al., 2009). Igneous rocks that experienced extensive Hg degassing during magma evolution have low Hg content and heavier δ^{202}Hg values

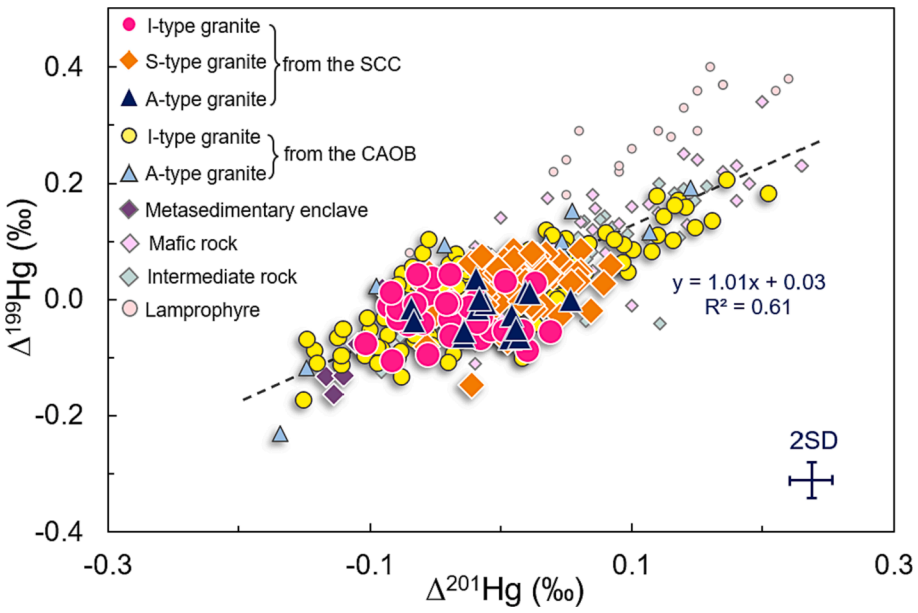

Fig. 6. Plot of Δ^{201}Hg versus Δ^{199}Hg for the studied granites (this study; Deng et al., 2022a)**, metasedimentary enclaves** (this study)**, lamprophyre** (Wang et al., 2021)**, mafic and intermediate rocks** (Geng et al., 2018; Moynier et al., 2020, 2021; Deng et al., 2022a; Yin et al., 2022).

Table 2
Mass balance model for Hg in the upper continental crust (UCC).

Rock units	Proportion in the UCC (%)[a]	Average Hg content (ppb)	Hg in the UCC (%)	Average δ^{202}Hg (‰)[d]	Average Δ^{199}Hg (‰)[d]
Sedimentary rocks	14	62.4[b]	64.95	−1.09 ± 1.46	0.04 ± 0.22
Granites	25	7.88 ± 16.5[c]	14.65	−0.96 ± 1.82	0.01 ± 0.13
Granodiorites	20	6.24 ± 9.52[c]	9.28	−1.04 ± 2.27	0.00 ± 0.14
Tonalites	5	6.58 ± 8.18[c]	2.45	−2.38 ± 1.74	0.07 ± 0.16
Gabbros	6	8.65 ± 19.0[c]	3.86	−2.27 ± 1.64	0.05 ± 0.13
Metamorphic rocks	30	2.16 ± 4.82[c]	4.82	−1.13 ± 1.30	−0.06 ± 0.28
UCC[e]	100	13.5 ± 17.8[c]	100	−1.15 ± 1.01	0.03 ± 0.15

[a] Division of major rock units in the UCC and their proportion are from Wedepohl (1995).

[b] Average Hg content of sedimentary rocks (n = 4500) is from Grasby et al. (2019).

[c] Average Hg contents of granites, granodiorites, tonalites, gabbros, and metamorphic rocks are calculated based on this study and previous data (Table S3).

[d] The average δ^{202}Hg, Δ^{199}Hg, and 2SD of sedimentary rocks (n = 1860, Table S4), granites (n = 204, Table S2), granodiorites (n = 44, Table S2), tonalites (n = 31, Table S4), gabbros (n = 19, Table S4), and metamorphic rocks (n = 35, Table S4) are based on this study and previous data.

[e] The weighted average δ^{202}Hg, Δ^{199}Hg, and 2SD of UCC is derived from mass balance calculations, using the following equation: the weighted average of $\delta^{202}Hg = \sum(\delta^{202}Hg_{rock\ unit} \times Hg\%)$, the weighted average of $\Delta^{199}Hg = \sum(\Delta^{199}Hg_{rock\ unit} \times Hg\%)$, 2SD of weighted average $= \sqrt{\sum(2SD_{rock\ unit} \times Hg\%)^2}$, where Hg% is Hg proportion of each rock unit in the UCC.

(Moynier et al., 2020; Deng et al., 2022a). The relatively lower δ^{202}Hg values of granites from the CAOB than from the SCC (Fig. 4) suggest a higher degree of Hg degassing for the SCC granites. However, the relatively higher THg contents of granites from the SCC than those from the CAOB contradict this possibility. In addition, the lack of correlations between δ^{202}Hg and magma differentiation indices (SiO_2, MgO; Fig. 3) suggests that significant Hg-MDF is unlikely to occur during the fractional crystallization of silicate minerals (Tian et al., 2022).

The distinct δ^{202}Hg composition of granites from the SCC and CAOB could also reflect the differences in their magma sources. Granites from the CAOB mostly exhibit positive $\varepsilon_{Hf}(t)$ values (0 to 10; Gou et al., 2019a, 2019b), implying that they formed by partial melting of the juvenile mafic lower crust (Deng et al., 2022a, and references therein), whereas granites from the SCC typically display negative $\varepsilon_{Hf}(t)$ (−16 to −3.1, Table 1) indicative of ancient crustal materials in their magma source (Li et al., 2007; Qi et al., 2007; Zhao et al., 2012a, 2013). Therefore, we suggest that the source composition could be a primary factor causing the large Hg isotopic heterogeneity between the SCC and CAOB granites.

5.3. *Hg-MIF signals unravel source mixing or MASH processes in the deep crust*

Diagenesis, metamorphism, and magmatic processes do not trigger large apparent Hg-MIF (Moynier et al., 2020; Chen et al., 2022; Yin et al., 2022) and therefore Δ^{199}Hg values can provide direct constraints on the Hg source. The studied S-type granites have Δ^{199}Hg values of −0.15 to 0.09 ‰, which is consistent with their sedimentary protoliths (−0.16 to 0.02 ‰), indicating that partial melting of these sedimentary protoliths provided the major Hg source for the studied S-type granites. Although large Δ^{199}Hg variation (−0.46 to 0.57 ‰; Table S4) has been reported in sedimentary rocks, sediments deposited in nearshore settings exhibit a smaller Δ^{199}Hg range of −0.2 to 0.1 ‰ (Yin et al., 2015, 2018; Meng et al., 2019) due to mixing of marine- and terrestrial-derived Hg. Herein, we speculate that the relatively small Δ^{199}Hg variation of our studied S-type granites may result from the efficient mixing of source materials in nearshore settings.

The I- and A-type granites studied have smaller Δ^{199}Hg ranges between −0.11 to 0.04 ‰ and −0.07 to 0.04 ‰, respectively (Fig. 4). These values are generally in line with previous results (mostly within −0.10 to 0.10 ‰) on mafic to intermediate rocks (Moynier et al., 2020, 2021; Deng et al., 2022a), supporting that these rocks were derived mainly from partial melting of igneous precursors. Previous studies indicate

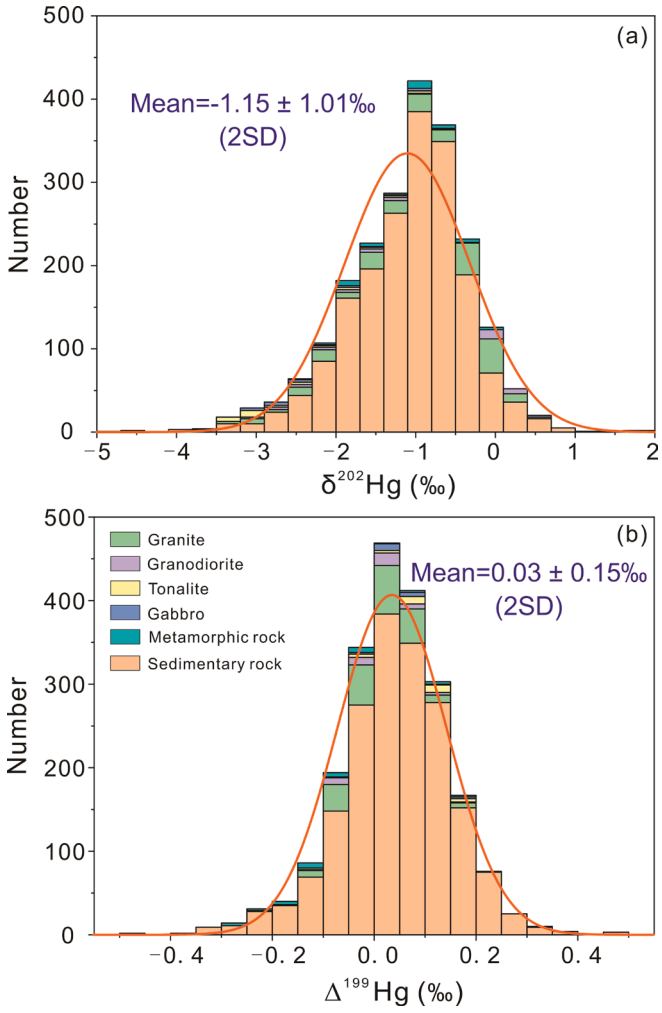

Fig. 7. Histograms of (a) δ^{202}Hg and (b) Δ^{199}Hg values of upper crustal rocks measured in this study (Supplementary Table S2) and previous studies (Supplementary Table S4). Both the δ^{202}Hg and Δ^{199}Hg values of upper crustal rocks show Gaussian distributions and yielded weighted averages of δ^{202}Hg of −1.20 ± 0.80 ‰ (2SD) and Δ^{199}Hg of 0.04 ± 0.12 ‰ (2SD) for the UCC. The orange line represents the fitted Gaussian curve.

that the source of the studied I- and A-type granites was ancient basement rocks rather than differentiates from mantle-derived mafic magmas (Zhao et al., 2012a, 2013; Li et al., 2007). The near-zero Δ^{199}Hg values of the studied I- and A-type granites are, therefore, unlikely inherited from the mantle, but from either (1) an intracrustal magma source that has a near-zero Δ^{199}Hg signature, or (2) a well-mixed source of components with complementary Δ^{199}Hg signals that average to near zero. Previous studies on bulk rock Sr-Nd and zircon Hf-O isotopes suggest that the studied I- and A-type granites were mainly derived from Paleoproterozoic mafic-intermediate igneous protoliths, with different degrees of contributions from sedimentary material and/or mantle-derived magma (Li et al., 2007, 2009; Zhao et al., 2012a, 2013). Thus, the mixing of deep-seated mafic-intermediate igneous material, sedimentary material, and/or mantle-derived magma during large-scale MASH processes (melting/assimilation/storage/homogenization; Hildreth, 1981) in the lower and middle crust could be a mechanism to explain the near-zero Δ^{199}Hg values for I- and A-type granites.

5.4. Hg isotopic composition of the upper continent crust

Our results, combined with previously reported data for upper crustal rocks, suggest that the UCC has heterogeneous Hg isotopic compositions with a range of −4.40 to 0.47 ‰ for δ^{202}Hg and −0.46 to 0.33 ‰ for Δ^{199}Hg (Table S2 and S4). When plotting these data on a histogram, they display Gaussian distribution characteristics with δ^{202}Hg peak of around −1.1 ‰ and Δ^{199}Hg peak of ~0.2 ‰ (Fig. 7). Similar to the previous studies on Mg and K isotopes (Li et al., 2010; Huang et al., 2020), the weighted average Hg isotopic composition of the UCC can be estimated based on the proportion of major rock units in the UCC, i.e., 14 % sediments, 25 % granite, 20 % granodiorite, 5 % tonalite, 6 % gabbro, and 30 % metamorphic rocks (Wedepohl, 1995), and their average δ^{202}Hg and Δ^{199}Hg values. According to this study and literature data (Supplementary Table S4), the mean δ^{202}Hg values of sedimentary rock, granite, granodiorite, tonalite, gabbro, and metamorphic rocks are calculated to be −1.09 ± 1.46 ‰ (2SD; n = 1860), −0.96 ± 1.82 ‰ (2SD; n = 204), −1.04 ± 2.27 ‰ (2SD; n = 44), −2.38 ± 1.74 ‰ (2SD; n = 31), −2.27 ± 1.64 ‰ (2SD; n = 19), and −1.13 ± 1.30 ‰ (2SD; n = 35), respectively, and the mean Δ^{199}Hg values are 0.04 ± 0.22 ‰ (2SD; n = 1860), 0.01 ± 0.13 ‰ (2SD; n = 204), 0.00 ± 0.14 ‰ (2SD; n = 44), 0.07 ± 0.16 ‰ (2SD; n = 31), 0.05 ± 0.13 ‰ (2SD; n = 19), and −0.06 ± 0.28 ‰ (2SD; n = 35), respectively (Table 2). Weighting the average Hg isotopic composition of the abovementioned six rock units by their estimated proportion and their average Hg content, the average δ^{202}Hg and Δ^{199}Hg compositions of the UCC are estimated to be −1.15 ± 1.01 ‰ (2SD) and 0.03 ± 0.15 ‰ (2SD), respectively (Fig. 7; Table 2), which can be viewed as a preliminary estimation of the Hg isotopic compositions of the UCC. Unless some portions of isotopically fractionated sediments are removed from the UCC, mass balance in Hg isotopes should constrain the average δ^{202}Hg and Δ^{199}Hg of all sedimentary rocks to be close to the corresponding values of igneous rocks, as all sedimentary rocks ultimately originated from igneous rocks. Granite, granodiorite, tonalite, and gabbro as a whole show mean δ^{202}Hg and Δ^{199}Hg values of −1.19 ± 2.13 ‰ (2SD; n = 298) and 0.02 ± 0.14 ‰ (2SD; n = 298), respectively, which are consistent with the mean values of sedimentary rocks (δ^{202}Hg = −1.09 ± 1.46 ‰, Δ^{199}Hg = 0.04 ± 0.22 ‰, 2SD; n = 1860), demonstrating the reliability of our estimate.

Compared to the mantle (δ^{202}Hg: −1.7 ± 1.2 ‰, Δ^{199}Hg: 0.00 ± 0.10 ‰, 2SD; Moynier et al., 2021), the UCC has an isotopically heavier δ^{202}Hg composition, but similar Δ^{199}Hg composition (Fig. 8). This indicates that there is significant Hg-MDF during the formation and differentiation of continental crust, but limited Hg-MIF. Preferential loss of lighter δ^{202}Hg during crust-mantle differentiation and intracrustal magmatic processes could be the reason causing such a large δ^{202}Hg difference between the UCC and the mantle. The detailed mechanism for this Hg-MDF is worthy of further investigation.

6. Conclusion

The main conclusions of this work are: (1) The Hg abundance of the upper continental crust is estimated to be 13.5 ± 17.8 ppb; (2) Compared to their sedimentary protoliths (δ^{202}Hg = −2.03 to −0.91 ‰, Δ^{199}Hg = −0.16 to 0.02 ‰), the studied S-type granites have higher δ^{202}Hg (−0.58 to 0.00 ‰) but similar Δ^{199}Hg values (−0.15 to 0.09 ‰), providing new evidence that magmatic processes lead to significant Hg-MDF but not Hg-MIF; (3) Source composition is an important factor causing the δ^{202}Hg variation between the granites of the South China Craton and the Central Asian Orogenic Belt, and the variable Δ^{199}Hg signals imply effective source mixing or MASH processes in deep crust; (4) The upper continental crust has a heterogeneous Hg isotopic composition with a weighted average δ^{202}Hg of −1.15 ± 1.01 ‰ (2SD) and Δ^{199}Hg of 0.03 ± 0.15 ‰ (2SD).

Declaration of Competing Interest

The authors declare that they have no known competing financial interests or personal relationships that could have appeared to influence the work reported in this paper.

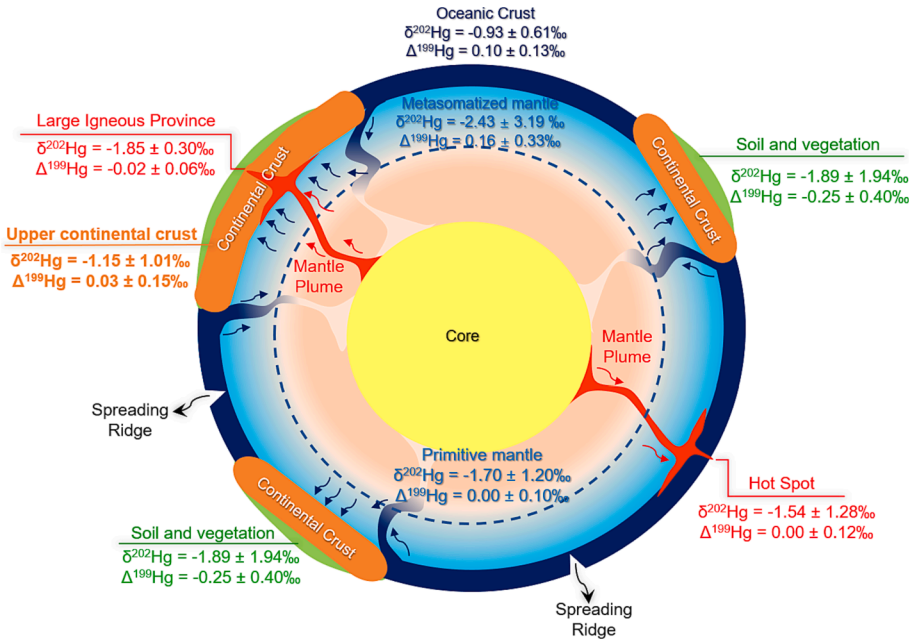

Fig. 8. A conceptual model showing Hg isotopic characteristics of the main layers of the Earth and the possible Hg cycle between different layers (not to scale). Plume-related volcanism (red-shaded areas) releases large amounts of Hg with near-zero Δ^{199}Hg values (red arrows) to Earth's surface. This Hg undergoes global transport and Hg(II) photoreduction processing on Earth's surface, leading to positive Δ^{199}Hg values in the oceanic system (dark blue shaded area) and negative Δ^{199}Hg in the terrestrial system (light green shaded area). Subduction of oceanic plate delivers large amounts of marine Hg into the mantle (dark blue arrows), causing the subduction-related fluid metasomatized mantle with positive Δ^{199}Hg (light blue shaded areas). The Hg isotopic composition of the primitive mantle is from Moynier et al. (2021). The average δ^{202}Hg and Δ^{199}Hg values of soil and vegetation were calculated based on previously published data (Biswas et al., 2008; Demers et al., 2013; Yin et al., 2013; Jiskra et al., 2015; Yu et al., 2016; Zheng et al., 2016; Obrist et al., 2017; Woerndle et al., 2018; Liu et al., 2019; Sonke et al., 2023). The δ^{202}Hg and Δ^{199}Hg values of the metasomatized mantle were calculated based on the data of lamprophyres (Wang et al., 2021). The δ^{202}Hg and Δ^{199}Hg values of oceanic crust and large igneous province were calculated based on the data of mid-ocean ridge basalts (Yin et al., 2022) and continental flood basalts (Yin et al., 2022), respectively. The δ^{202}Hg and Δ^{199}Hg values of hot spot were calculated based on the data of ocean island basalts (Moynier et al., 2021; Yin et al., 2022).

Data availability

Data are available through Mendeley Data at https://doi.org/10.17632/gtxnrc5m3d.1.

Acknowledgement

We thank the Editors Jeffrey Catalano and Shengao Liu for their efficient handling and the three reviewers for their very insightful comments that greatly improved the paper. This work was supported by the Natural Science Foundation of China (41873047), Guizhou Provincial 2021 Science and Technology Subsidies (GZ2021SIG), and the Chinese Academy of Sciences through the Hundred Talent Plan.

Appendix A. Supplementary material

The supplementary materials include the detailed petrology and geochemical description of our studied six granitic batholiths/complexes and metasedimentary enclaves (Text S1), representative field and micrographs of studied granites (Figure S1), whole-rock major and trace element composition of three types of granites (Table S1), Hg concentration and isotopic compositions of three types of granites and metasedimentary enclaves (Table S2), Hg concentration of upper crustal rocks (Table S3), and Hg isotopic composition of upper crustal rocks (Table S4). Supplementary material to this article can be found online at https://doi.org/10.1016/j.gca.2023.09.019.

References

Bergquist, B.A., Blum, J.D., 2007. Mass-dependent and -independent fractionation of Hg isotopes by photoreduction in aquatic systems. Science 318, 417–420.

Bergquist, B.A., Blum, J.D., 2009. The odds and evens of mercury isotopes: Applications of mass-dependent and mass-independent isotope fractionation. Elements 5, 353–357.

Biswas, A., Blum, J.D., Bergquist, B.A., Keeler, G.J., Xie, Z., 2008. Natural mercury isotope variation in coal deposits and organic soils. Environ. Sci. Tech. 42 (22), 8303–8309.

Blum, J.D., Bergquist, B.A., 2007. Reporting of variations in the natural isotopic composition of mercury. Anal. Bioanal. Chem. 388, 353–359.

Blum, J.D., Sherman, L.S., Johnson, M.W., 2014. Mercury isotopes in earth and environmental sciences. Annu. Rev. Earth Planet. Sci. 42, 249–269.

Canil, D., Crockford, P.W., Rossin, R., Telmer, K., 2015. Mercury in some arc crustal rocks and mantle peridotites and relevance to the moderately volatile element budget of the Earth. Chem. Geol. 396, 134–142.

Chappell, B., White, A., 1974. Two contrasting granite types. Pacif. Geol. 8, 173–174.

Chen, D., Ren, D., Deng, C., Tian, Z., Yin, R., 2022. Mercury loss and isotope fractionation during high-pressure and high-temperature processing of sediments: Implication for the behaviors of mercury during metamorphism. Geochim. Cosmochim. Acta 334, 231–240.

Collins, W.J., Beams, S.D., White, A.J.R., Chappell, B.W., 1982. Nature and origin of A-type granites with particular reference to southeastern Australia. Contrib. Miner. Petrol. 80, 189–200.

Demers, J.D., Blum, J.D., Zak, D.R., 2013. Mercury isotopes in a forested ecosystem: Implications for air-surface exchange dynamics and the global mercury cycle. Glob. Biogeochem. Cycles 27, 222–238.

Deng, C., Sun, G., Rong, Y., Sun, R., Sun, D., Lehmann, B., Yin, R., 2021. Recycling of mercury from the atmosphere-ocean system into volcanic-arc–associated epithermal gold systems. Geology 49, 309–313.

Deng, C., Gou, J., Sun, D., Sun, G., Tian, Z., Lehmann, B., Moynier, F., Yin, R., 2022a. Mercury isotopic composition of igneous rocks from an accretionary orogen: Implications for lithospheric recycling. Geology 50 (9), 1001–1006.

Deng, C., Zhang, J., Hu, R., Luo, K., Zhu, Y., Yin, R., 2022b. Mercury isotope constraints on the genesis of late Mesozoic Sb deposits in South China. Sci. China, Ser. D Earth Sci. 65, 269–281.

Estrade, N., Carignan, J., Sonke, J.E., Donard, O.F.X., 2009. Mercury isotope fractionation during liquid–vapor evaporation experiments. Geochim. Cosmochim. Acta 73, 2693–2711.

Estrade, N., Carignan, J., Sonke, J.E., Donard, O.F.X., 2010. Measuring Hg isotopes in bio-geo-environmental reference materials. Geostand. Geoanal. Res. 34, 79–93.

Gao, S., Luo, T.-C., Zhang, B.-R., Zhang, H.-F., Han, Y.-W., Zhao, Z.-D., Hu, Y.-K., 1998. Chemical composition of the continental crust as revealed by studies in East China. Geochim. Cosmochim. Acta 62, 1959–1975.
Geng, H., Yin, R., Li, X., 2018. An optimized protocol for high precision measurement of Hg isotopic compositions in samples with low concentrations of Hg using MC-ICP-MS. J. Anal. At. Spectrom 33, 1932–1940.
Ghosh, S., Schauble, E., Couloume, G., Blum, J., Bergquist, B.A., 2013. Estimation of nuclear volume dependent fractionation of mercury isotopes in equilibrium liquid–vapor evaporation experiments. Chem. Geol. 336, 5–12.
Gou, J., Sun, D.-Y., Qin, Z., 2019a. Late Jurassic-Early Cretaceous tectonic evolution of the Great Xing'an Range: geochronological and geochemical evidence from granitoids and volcanic rocks in the Erguna Block, NE China. Int. Geol. Rev. 61, 1842–1863.
Gou, J., Sun, D.-Y., Yang, D.-G., Tang, Z.-Y., Mao, A.-Q., 2019b. Late Palaeozoic igneous rocks of the Great Xing'an Range, NE China: the Tayuan example. Int. Geol. Rev. 61, 314–340.
Grasby, S.E., Them, T.R., Chen, Z., Yin, R., Ardakani, O.H., 2019. Mercury as a proxy for volcanic emissions in the geologic record. Earth Sci. Rev. 196, 102880.
Hans Wedepohl, K., 1995. The composition of the continental crust. Geochim. Cosmochim. Acta 59, 1217–1232.
Hildreth, W., 1981. Gradients in silicic magma chambers: implications for lithospheric magmatism. J. Geophys. Res. Solid Earth 86, 10153–10192.
Hoefs, J., 2021. Stable Isotope Geochemistry, ninth ed. Springer, Berlin.
Hsieh, P.-S., Chen, C.-H., Yang, H.-J., Lee, C.-Y., 2008. Petrogenesis of the Nanling mountains granites from South China: Constraints from systematic apatite geochemistry and whole-rock geochemical and Sr–Nd isotope compositions. J. Asian Earth Sci. 33, 428–451.
Huang, Q., Liu, Y., Chen, J., Feng, X., Huang, W., Yuan, S., Cai, H., Fu, X., 2015. An improved dual-stage protocol to pre-concentrate mercury from airborne particles for precise isotopic measurement. J. Anal. At. Spectrom 30, 957–966.
Huang, T.-Y., Teng, F.-Z., Rudnick, R.L., Chen, X.-Y., Hu, Y., Liu, Y.-S., Wu, F.-Y., 2020. Heterogeneous potassium isotopic composition of the upper continental crust. Geochim. Cosmochim. Acta 278, 122–136.
Jiskra, M., Wiederhold, J.G., Skyllberg, U., Kronberg, R.-M., Hajdas, I., Kretzschmar, R., 2015. Mercury deposition and re-emission pathways in Boreal forest soils investigated with Hg isotope signatures. Environ. Sci. Tech. 49, 7188–7196.
Johnson, C.M., Beard, B.L., Albarède, F., 2018. Geochemistry of Non-traditional Stable Isotopes. Mineralogical Society of America and the Geochemical Society, Washington.
Kim, J., Lim, D., Jeong, D., Xu, Z.K., Kim, H., Kim, J., Kim, D., 2022. Mercury (Hg) geochemistry of mid-ocean ridge sediments on the Central Indian Ridge: Chemical forms and isotopic composition. Chem. Geol. 604, 120942.
Lan, H., Ling, H., Chen, W., Liu, J., Ouyang, P., 2018. Study on petrogenesis and uranium mineralization potential of eastern sanjiangkou granitic pluton. Geol. J. China Univ. 24, 172–184.
Lechler, P.J., Desilets, M.O., 1987. A review of the use of loss on ignition as a measurement of total volatiles in whole-rock analysis. Chem. Geol. 63, 341–344.
Li, X.-H., Li, Z.-X., Li, W.-X., Liu, Y., Yuan, C., Wei, G., Qi, C., 2007. U-Pb zircon, geochemical and Sr–Nd–Hf isotopic constraints on age and origin of Jurassic I- and A-type granites from central Guangdong, SE China: A major igneous event in response to foundering of a subducted flat-slab? Lithos 96, 186–204.
Li, X., Li, W., Wang, X., Li, Q., Liu, Y., Tang, G., 2009. Role of mantle-derived magma in genesis of early Yanshanian granites in the Nanling Range, South China: in situ zircon Hf-O isotopic constraints. Sci. China Ser. D Earth Sci. 52, 1262–1278.
Li, W.-Y., Teng, F.-Z., Ke, S., Rudnick, R.L., Gao, S., Wu, F.-Y., Chappell, B.W., 2010. Heterogeneous magnesium isotopic composition of the upper continental crust. Geochim. Cosmochim. Acta 74, 6867–6884.
Liu, H.W., Shao, J.J., Yu, B., Liang, Y., Duo, B., Fu, J.J., Yang, R.Q., Shi, J.B., Jiang, G.B., 2019. Mercury isotopic compositions of mosses, conifer needles, and surface soils: Implications for mercury distribution and sources in Shergyla Mountain, Tibetan Plateau. Ecotoxicol. Environ. Saf. 172, 225–231.
Ma, L.Y., Liu, S.S., Fu, J.M., Cheng, S.B., Lu, Y.Y., Mei, Y.P., 2016. Petrogenesis of the Tashan-Yangmingshan granite batholith: constraint from zircon U-Pb age, geochemistry, and Sr-Nd isotopes. Acta Geol. Sin. 90, 284–303.
Maniar, P.D., Piccoli, P.M., 1989. Tectonic discrimination of granitoids. Geol. Soc. Am. Bull. 101, 635–643.
Meng, M., Sun, R.B., Liu, H.W., Yu, B., Yin, Y.G., Hu, L.G., Shi, J.B., Jiang, G.B., 2019. An integrated model for input and migration of mercury in Chinese coastal sediments. Environ. Sci. Tech. 53, 2460–2471.
Middlemost, E.A.K., 1994. Naming materials in the magma/igneous rock system. Earth Sci. Rev. 37, 215–224.
Moynier, F., Chen, J., Zhang, K., Cai, H., Wang, Z., Jackson, M.G., Day, J.M.D., 2020. Chondritic mercury isotopic composition of Earth and evidence for evaporative equilibrium degassing during the formation of eucrites. Earth Planet. Sci. Lett. 551, 116544.
Moynier, F., Jackson, M.G., Zhang, K., Cai, H., Halldórsson, S.A., Pik, R., Day, J.M.D., Chen, J., 2021. The mercury isotopic composition of Earth's mantle and the use of mass independently fractionated Hg to test for recycled crust. Geophys. Res. Let.t 48.
Nesbitt, H.W., Young, G.M., 1984. Prediction of some weathering trends of plutonic and volcanic rocks based on thermodynamic and kinetic considerations. Geochim. Cosmochim. Acta 48 (7), 1523–1534.
Obrist, D., Agnan, Y., Jiskra, M., Olson, C.L., Colegrove, D.P., Hueber, J., Moore, C., Sonke, J.E., Helmig, D., 2017. Tundra uptake of atmospheric elemental mercury drives Arctic mercury pollution. Nature 547 (7662), 201–204.
Qi, C., Deng, X., Li, W., Li, X., Yang, Y., Xie, L., 2007. Origin of the Darongshan-Shiwandashan S-type granitoid belt from southeastern Guangxi: geochemical and Sr-Nd-Hf isotopic constraints. Acta Petrol. Sin. 23, 403–412.
Qi, L., Hu, J., Grégoire, D.C., 2000. Determination of trace elements in granites by inductively coupled plasma mass spectrometry. Talanta 51, 507–513.
Rudnick, R.L., Gao, S., 2003. Composition of the continental crust. In: Holland, H.D., Turekian, K.K. (Eds.), Treatise on Geochemistry. Elsevier-Pergamon, Oxford, pp. 1–64.
Shaw, D.M., Dostal, J., Keays, R.R., 1976. Additional estimates of continental surface Precambrian shield composition in Canada. Geochim. Cosmochim. Acta 40, 73–83.
Shu, L., Yao, J., Wang, B., Faure, M., Charvet, J., Chen, Y., 2021. Neoproterozoic plate tectonic process and Phanerozoic geodynamic evolution of the South China Block. Earth Sci. Rev. 216, 103596.
Sonke, J., Shevchenko, V., Prunier, J., Sun, R., Prokushkin, A., Pokrovsky, O., 2023. Mercury stable isotope composition of lichens and mosses from northern Eurasia. ACS Earth Space Chem. 7 (1), 204–211.
Štrok, M., Baya, P.A., Hintelmann, H., 2015. The mercury isotope composition of Arctic coastal seawater. C.R. Geosci. 347, 368–376.
Sun, G., Sommar, J., Feng, X., Lin, C.-J., Ge, M., Wang, W., Yin, R., Fu, X., Shang, L., 2016. Mass-dependent and -independent fractionation of mercury isotope during gas-phase oxidation of elemental mercury vapor by atomic Cl and Br. Environ. Sci. Tech. 50 (17), 9232–9241.
Taylor, S.R., 1964. Abundance of chemical elements in the continental crust: a new table. Geochim. Cosmochim. Acta 28, 1273–1285.
Tian, Z., Leng, C., Deng, C., Zhang, X., Chen, D., Gao, L., Wang, X., Yin, R., 2022. Mercury isotopes as a useful tracer of magma sources: An example from the Daocheng-Cuojiaoma batholith, eastern Tibetan Plateau. Chem. Geol. 606, 120974.
Wang, X., Deng, C., Yang, Z., Zhu, J.-J., Yin, R., 2021. Oceanic mercury recycled into the mantle: Evidence from positive Δ^{199}Hg in lamprophyres. Chem. Geol. 584, 120505.
Whalen, J.B., Currie, K.L., Chappell, B.W., 1987. A-type granites: geochemical characteristics, discrimination and petrogenesis. Contrib. Miner. Petrol.. 95, 407–419.
Woerndle, G.E., Tsz-Ki Tsui, M., Sebestyen, S.D., Blum, J.D., Nie, X., Kolka, R.K., 2018. New insights on ecosystem mercury cycling revealed by stable isotopes of mercury in water flowing from a headwater peatland catchment. Environ. Sci. Tech. 52 (4), 1854–1861.
Yin, R., Feng, X., Meng, B., 2013. Stable mercury isotope variation in rice plants (oryza sativa L.) from the Wanshan mercury mining district, SW China. Environ. Sci. Technol. 47, 2238–2245.
Yin, R., Feng, X., Chen, B., Zhang, J., Wang, W., Li, X., 2015. Identifying the sources and processes of mercury in subtropical estuarine and ocean sediments using Hg isotopic composition. Environ. Sci. Tech. 49, 1347–1355.
Yin, R., Krabbenhoft, D.P., Bergquist, B.A., Zheng, W., Lepak, R.F., Hurley, J.P., 2016. Effects of mercury and thallium concentrations on high precision determination of mercury isotopic composition by Neptune Plus multiple collector inductively coupled plasma mass spectrometry. J. Anal. At. Spectrom 31, 2060–2068.
Yin, R., Guo, Z., Hu, L., Liu, W., Hurley, J.P., Lepak, R.F., Lin, T., Feng, X., Li, X., 2018. Mercury inputs to Chinese marginal seas: Impact of industrialization and development of China. J. Geophys. Res. Oceans 123, 5599–5611.
Yin, R., Chen, D., Pan, X., Deng, C., Chen, L., Song, X., Yu, S., Zhu, C., Wei, X., Xu, Y., Feng, X., Blum, J.D., Lehmann, B., 2022. Mantle Hg isotopic heterogeneity and evidence of oceanic Hg recycling into the mantle. Nat. Commun. 13, 948.
Yu, B., Fu, X., Yin, R., Zhang, H., Wang, X., Lin, C.J., Feng, X., 2016. Isotopic composition of atmospheric mercury in China: new evidence for sources and transformation processes in air and in vegetation. Environ. Sci. Tech. 50 (17), 9262–9269.
Yuan, J.J., Liu, Y., Chen, S., Peng, X.T., Li, Y.F., Li, S.J., Zhang, R., Zheng, W., Chen, J.B., Sun, R.Y., Heimbürger-Boavida, L.E., 2023. Mercury isotopes in deep-sea epibenthic biota suggest limited Hg transfer from photosynthetic to chemosynthetic food webs. Environ. Sci. Tech. 57, 6550–6562.
Zambardi, T., Sonke, J.E., Toutain, J.P., Sortino, F., Shinohara, H., 2009. Mercury emissions and stable isotopic compositions at Vulcano Island (Italy). Earth Planet. Sci. Lett. 277, 236–243.
Zhai, M., 2015. Precambrian Geology of China. Springer, Berlin.
Zhang, L., Chen, Z.Y., Li, S.R., Santosh, M., Huang, G.L., Tian, Z.J., 2017. Isotope geochronology, geochemistry, and mineral chemistry of the U-bearing and barren granites from the Zhuguangshan complex, South China: Implications for petrogenesis and uranium mineralization. Ore Geol. Rev. 91, 1040–1065.
Zhao, L., Guo, F., Fan, W., Li, C., Qin, X., Li, H., 2012b. Origin of the granulite enclaves in Indo-Sinian peraluminous granites, South China and its implication for crustal anatexis. Lithos 150, 209–226.
Zhao, K.-D., Jiang, S.-Y., Yang, S.-Y., Dai, B.-Z., Lu, J.-J., 2012a. Mineral chemistry, trace elements and Sr–Nd–Hf isotope geochemistry and petrogenesis of Cailing and Furong granites and mafic enclaves from the Qitianling batholith in the Shi-Hang zone, South China. Gondwana Res. 22, 310–324.
Zhao, K.-D., Jiang, S.-Y., Sun, T., Chen, W.-F., Ling, H.-F., Chen, P.-R., 2013. Zircon U-Pb dating, trace element and Sr–Nd–Hf isotope geochemistry of Paleozoic granites in the Miao'ershan–Yuechengling batholith, South China: Implication for petrogenesis and tectonic–magmatic evolution. J. Asian Earth Sci. 74, 244–264.
Zhao, G.C., Wang, Y.J., Huang, B.C., Dong, Y.P., Li, S.Z., Zhang, G.W., Yu, S., 2018. Geological reconstructions of the East Asian blocks: From the breakup of Rodinia to the assembly of Pangea. Earth Sci. Rev. 216, 262–286.
Zheng, W., Obrist, D., Weis, D., Bergquist, B.A., 2016. Mercury isotope compositions across North American forests. Glob. Biogeochem. Cycles. 30, 1475–1492.